

Research Article

Organic Material-Derived Activated Carbon for Eco-Friendly Mulberry Paper Supercapacitor

Yurim Han ,¹ Hyungsub Yoon ,² Jun Young Cheong ,³ and Byungil Hwang ¹

¹School of Integrative Engineering, Chung-Ang University, Seoul 06974, Republic of Korea

²Department of Intelligent Semiconductor Engineering, Chung-Ang University, Seoul 06974, Republic of Korea

³James Watt School of Engineering, University of Glasgow, Glasgow G12 8QQ, UK

Correspondence should be addressed to Jun Young Cheong; junyoung.cheong@glasgow.ac.uk and Byungil Hwang; bihwang@cau.ac.kr

Received 25 November 2024; Accepted 13 February 2025

Academic Editor: Amar Patil

Copyright © 2025 Yurim Han et al. International Journal of Energy Research published by John Wiley & Sons Ltd. This is an open access article under the terms of the Creative Commons Attribution License, which permits use, distribution and reproduction in any medium, provided the original work is properly cited.

Paper has gained increasing attention as promising flexible substrate for deformable energy storage systems. However, since low mechanical strength and chemical resistance of commercial paper limited its practical application, mulberry paper (MP) has alternatively studied, which exhibits high holocellulose content, hydrophilicity, and strong bonding with active material. Herein, we prepared activated carbon (AC) using a one of common waste, orange peel (OP), and coated it on MP with additional coating of poly(3,4-ethylenedioxythiophene) polystyrene sulfonate (PEDOT:PSS), thereby, fabricating hybrid-coated MP for supercapacitor. The prepared AC exhibited enlarged surface area from 1.774 to 986.010 m²/g, and increased total pore volume of 0.639 cm³/g. Furthermore, additional coating of pseudocapacitive material enhanced electrochemical performance. Specific areal capacitance increased approximately 2.3 times, especially showing 78.95 ± 3.04 mF/cm² under scan rate of 100 mV/s. Moreover, fabricated electrode exhibited enhanced energy density of 3.01 μWh/cm² at current density of 0.5 mA/cm², thereby, complementing low energy density of electric double layer (EDL) capacitive material. This approach, which combines biomass-derived AC and MP with hybrid PEDOT:PSS coating, presents a promising pathway for next-generation sustainable energy storage systems.

Keywords: activated carbon; biomass; flexible electrode; hybrid coating; mulberry paper; supercapacitor

1. Introduction

As demand for wearable devices increases, flexible substrates have been actively studied for reliable use in electronic devices under deformable environments. Among these, paper is a promising substrate due to its light weight, cost effectiveness, abundance, and eco-friendliness. However, commercial paper, which has been generally used in previous research, has low mechanical strength and acid resistance, thereby, limiting its application. This is because stability under repetitive deformation and in the presence of acidic electrolytes is crucial for reliable operation of the flexible supercapacitor. Therefore, the traditional mulberry paper (MP), known as Hanji, has attracted increasing attention as a potential paper substrate. Because MP consists of longer and thicker fibers than

commercial paper, it exhibits excellent mechanical strength owing to enhanced van der Waals forces between fibers [1]. Furthermore, MP contains a holocellulose structure (a mixture of cellulose and hemicellulose) with abundant —OH groups, which strengthen the bonding between intertwined fibers by supplying numerous hydrogen-bonding sites and contributes to the excellent wettability of the MP, compared to commercial paper, polyethylene terephthalate, and cellulose filter [1–3], thereby, allowing simple and large-scale solution coating [1]. In addition, the —OH groups also participate in bonding with coating materials and contribute to strong adhesion with active materials, as confirmed by previous studies [4, 5]. The other primary structure of paper, lignin, is a component of the plant cell wall, and the durability of paper depends on the lignin content. Thus, the low lignin content of MP relative to

commercial paper enhances the mechanical toughness of MP. Therefore, the high holocellulose and low lignin contents of MP provide it with both excellent mechanical strength and wettability, thereby, ensuring more reliable operation and adequate coating as a flexible substrate than other flexible substrates.

Although MP has notable advantages for use as a substrate for flexible energy storage systems, it requires coating with active materials due to its inherently insulating property. Activated carbon (AC) is a commonly-used electric double layer capacitor (EDLC) material, and includes carbon nanotubes (CNTs), graphene, and carbon black [6]. For practical application, this material must satisfy the following characteristics: (i) a high specific surface area (m^2/g) to ensure a high specific capacitance value, (ii) a low resistivity, and (iii) a well-adapted microtexture to allow good electrolyte accessibility into the inner surface of the electrode [7].

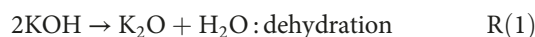
Conventional AC has a mesoporous structure, with pore diameters in the range of 2–50 nm, and exhibits a large surface area due to well-developed internal structure. Hence, when the electrode is coated with conductive carbon materials, charge accumulates at the electric double layer (EDL) via the electrostatic force to create a capacitance [6, 8]. Thus, AC has been largely used for EDLC applications involving porous carbon materials, for example, for catalyst supports, battery electrodes, and capacitors [9, 10]. Moreover, AC is most widely used for supercapacitor electrodes due to its low cost, high specific area, and good conductivity [11]. In particular, AC derived from biomass is more eco-friendly and cost-effective than commercial AC, especially regarding production processing and recycling [12]. Hence, as the exhaustion of fossil fuel becomes a serious problem [13], biomass has many advantages in terms of recycling, restoration, and consistent supply from natural sources. In addition, the intrinsic properties of biomass, including the presence of heteroatoms such as nitrogen (N), oxygen (O), and sulfur (S), greatly contribute to high electrode performance [14]. Moreover, biomass-derived ACs are recognized as electrode materials with superior potential due to their favorable physical/chemical properties, including chemical stability, low cost, scale-up capability, tunable microstructure, and various surface functional groups [15, 16].

Various types of ACs can be obtained, depending on the nature of the raw precursors, treatment conditions, and activating agent [17]. Hence, the choice of raw material and synthesis process are crucial factors for the preparation and properties of porous carbon [18]. Currently, materials of natural origin are often used as precursors in the synthesis of carbonaceous materials [19], so much research has been actively performed on biomass-derived AC from various sources such as rice husk [11], coconut shell [20], and reed straw [21]. In the present study, AC is prepared by using orange peel (OP), which has the potential to be a good precursor for the production of highly porous AC by simple methods. OP is a widely available and cost-effective material that is disposed of in large quantities in both households and industries. The sustainable supply of precursors from nature is significant not only from a large-scale and long-term perspective but also in terms of recycling waste into useful products for energy storage systems.

Notably, the combination of MP and biomass-derived AC provides significant eco-friendliness as a flexible energy storage system for wearable devices. Hence, an MP-based electrode is fabricated herein for use as a flexible supercapacitor. Further, after optimization of the AC coating, the electrochemical performance of the as-fabricated MP-based electrode is evaluated in areal metrics. In terms of thin-film electrode, the areal metrics are primarily recommended to avoid misleading exaggeration of gravimetric and volumetric capacitances due to its small mass and volume and to consider its practical application in micro/nano devices and flexible electronics in the real world. The results demonstrate that the as-prepared AC contributes to the enhancement of power density due to formation of EDL on its large surface area, while an additional coating of poly(3,4-ethylenedioxythiophene) polystyrene sulfonate (PEDOT:PSS), which was examined to exhibit synergistic effect with EDL capacitive materials [4, 22], increases the specific capacitance based on faradaic reaction. Thus, the coating of PEDOT:PSS, which is a representative pseudocapacitive material, complements the low energy density of the EDLC, while the AC contributes to overcoming the low capacity retention of the pseudocapacitor in actual device operation [23]. Overall, the present study demonstrates the possibility of developing next-generation eco-friendly energy-storage systems along with the recycling of biomass while providing enhanced electrochemical performance due to the hybrid coating of EDL and pseudocapacitive materials.

2. Experimental

2.1. Materials and Methods. Oranges were purchased at a local market in Korea, then peeled and dried in an oven for 24 h at 80°C for subsequent treatments. These included cleaning with hydrochloric acid (HCl; 9 M, Samchun), hydrothermal carbonization (HTC), vacuum filtration, and treatment with potassium hydroxide (KOH; 85%, Samchun). Thus, after drying, the OP was dipped in 1 M HCl solution for 12 h to remove any residues on the surface. After cleaning, washing, and drying, the mass of the OP was found to have decreased to 50% of its original value. The OP was then mixed with DI water in a mass ratio of 1:5 and transferred to a teflon container for HTC. The HTC was then performed for 2 h at 250°C in an autoclave (CUHTV-0050, Cuotalab), followed by vacuum filtration using a mixed cellulose membrane (MCE) filter (pore size: 20 μ m, Hyundai micro). The resulting HTC-OP sample was then subjected to KOH activation. For this procedure, a mixture of HTC-OP and 1 M KOH was magnetically stirred at 80°C for 1 h for solvent evaporation, then, transferred to an alumina boat and heated at 750°C for 2 h in a tubular furnace at a heating rate of 5°C/min to obtain the OP-derived AC (OPAC). KOH has been widely used as a cost-effective and less corrosive activation agent, producing AC with high surface area, uniform distribution of pore, and low environmental pollution [24–26]. The KOH activation generally follows the reaction sequence of R (1)–R (7):



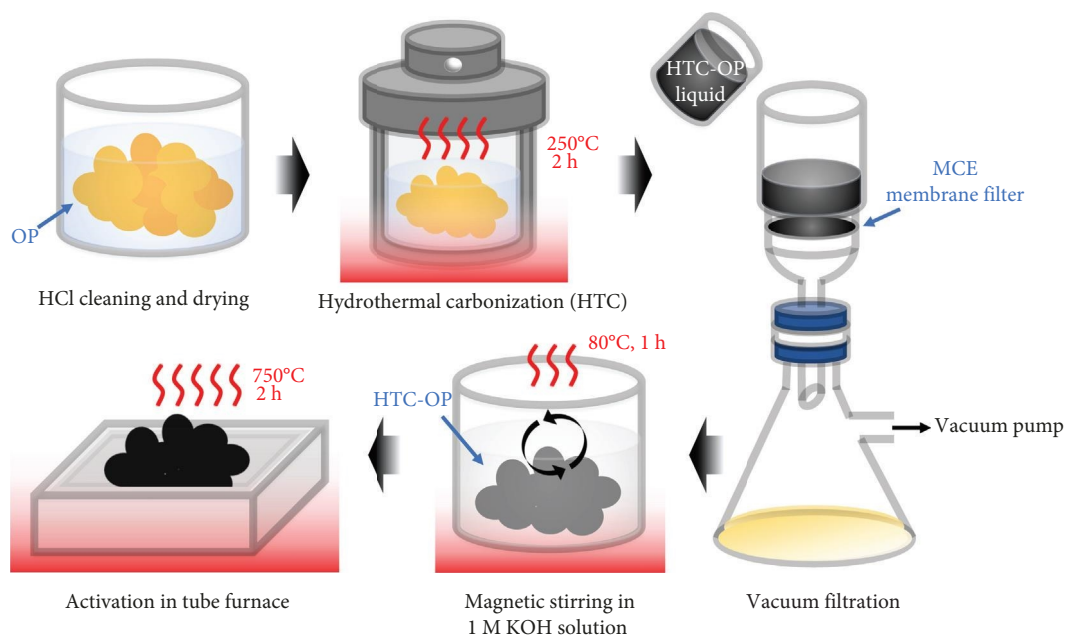
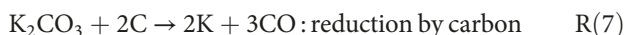
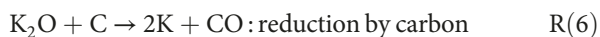
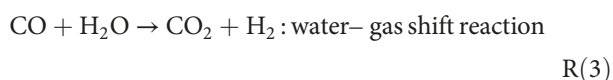


FIGURE 1: A schematic diagram showing the preparation of the orange peel-derived activated carbon (OPAC).



First, KOH, which plays key role in the chemical activation, is transformed into K_2O at 400°C by dehydration (R (1)) and then, water-gas reaction and water-gas shift reaction occur (R (2) and (3)). However, gasification alone is not enough to explain excessively porous structure of AC so that the additional mechanism occurs. At carbonization temperatures higher than 700°C , the metallic potassium was formed and by reduction with C and H_2 (R (5)–(7)) and penetrated into precursor. Therefore, the penetration of metallic potassium influences the formation of porous structure, contributing to high surface area. Finally, the activated OP was cleaned using HCl to remove any remaining KOH, and the resulting organic waste-derived product is designated hereafter as OPAC. The full preparation procedure is shown schematically in Figure 1.

The PEDOT:PSS/OPAC@MP electrode was fabricated via simple dip coating. For this procedure, the as-fabricated OPAC as the active material was dispersed along with CNTs (6A, JEIO) as a conductive additive in deionized (DI) water, with sodium dodecyl-benzenesulfonate (SDBS; Samchun) as the surfactant. A tip sonicator was used to prepare OPAC inks with various CNT:OPAC mass ratios of 1:0, 1:10, 1:20, and 1:30, wherein the masses

of CNTs and SDBS were fixed at 0.01 and 0.04 g, respectively. The resulting inks are designated as OPAC0, OPAC10, OPAC20, and OPAC30, respectively. Notably, OPAC0 does not contain any OPAC, serving as a control group. Meanwhile, 0.95 mL of the PEDOT:PSS (1.1 wt%, Sigma-Aldrich,) was further diluted in 4 g of DI water and 0.05 mL of ethylene glycol (EG; Sigma-Aldrich,) via magnetic stirring for further enhanced conductivity. The MP (thickness: $20\ \mu\text{m}$, Hanji-mall) substrates were dipped into the abovementioned OPAC inks for 15 s, and heated on a hotplate at 120°C for 10 min to obtain the electrodes designated OPAC0@MP, OPAC10@MP, OPAC20@MP, and OPAC30@MP, respectively. Subsequently, the OPAC20@MP electrode was dipped in the PEDOT:PSS solution for 15 s and subjected to the same heat treatment to obtain the PEDOT:PSS/OPAC@MP electrode. The entire electrode fabrication procedure is shown schematically in Figure 2. For fabrication of coin cell, the electrode was cut into circular shape with a radius of 0.6 cm, resulting in an electrode area of $1.131\ \text{cm}^2$.

2.2. Characterization and Measurement. The MP was characterized via field-emission scanning electron microscopy (FE-SEM; SIGMA 300, Carl Zeiss), rheometry (compac-100II, Sun Scientific) for tensile testing, drop-shape analysis (DSA 100, KRUSS) for contact angle measurement, and X-ray photoelectron spectroscopy (XPS; K-Alpha+, ThermoFisher Scientific) for the chemical composition. The tensile tests were repeated 10 times, and the average values were taken as the results. The as-prepared OPAC was characterized by FE-SEM with energy-dispersive X-ray spectroscopy (EDS), and by its Brunauer-Emmett-Teller (BET) isotherm to identify its pore structure, carbon content, and surface area. The PEDOT:PSS/OPAC@MP electrode was also characterized by FE-SEM to confirm proper coating of the active materials. For electrochemical measurement, a symmetric coin-cell system was employed using 1M sulfuric acid (H_2SO_4) solution

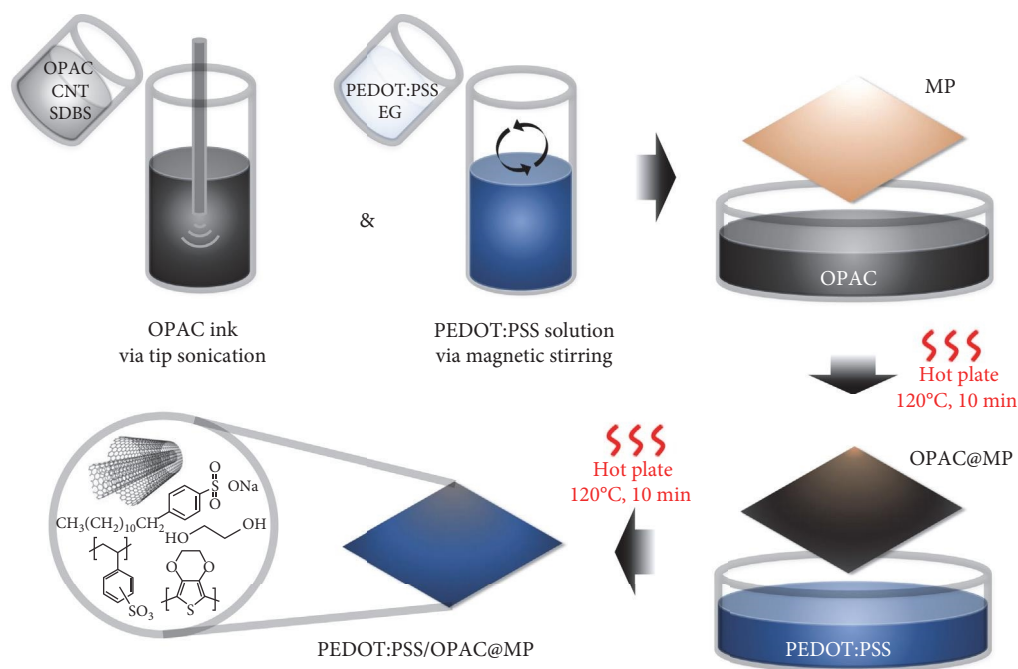


FIGURE 2: A schematic diagram showing the fabrication process of the PEDOT:PSS/OPAC@MP electrode. MP, mulberry paper; OPAC, orange peel-derived activated carbon; PEDOT, poly(3,4-ethylenedioxythiophene); PSS, polystyrene sulfonate.

(98%, Daejung) in DI water as an electrolyte. Cyclic voltammetry (CV) was conducted in the voltage range of 0–0.85 V (to prevent electrolysis of the DI water) at scan rates of 5, 10, 20, 50, 100, and 200 mV/s. The charge–discharge (CD) curves were obtained at current densities of 0.2, 0.5, 1.0, and 2.0 mA/cm². Every performance metric is calculated in areal term since areal performance is significant in practical application in micro/nano devices and wearable electronics. The specific capacitance (C_s) was calculated from the CV curve by using Equation (8):

$$C_s = \frac{\int I_m dV}{k\Delta V}, \quad (8)$$

where I_m is current density per unit area, which represents current (I) divided by electrode area (A); $\int I_m dV$ is the enclosed area of the CV curve, k is the scan rate, and ΔV is the voltage window. A and ΔV were considered fixed at 1.131 cm² and 0.85 V, respectively, throughout the experiment.

The specific capacitance (designated C_{CD}) was also calculated from the CD curve by using Equation (9):

$$C_{CD} = \frac{I_m \Delta t}{\Delta V}, \quad (9)$$

where Δt is the discharge time.

The energy density (E) was then calculated using Equation (10):

$$E = \frac{C_{CD}(\Delta V)^2}{2}, \quad (10)$$

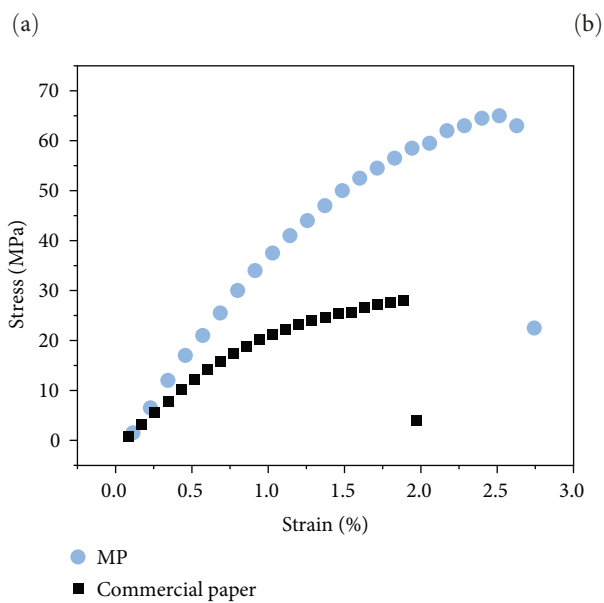
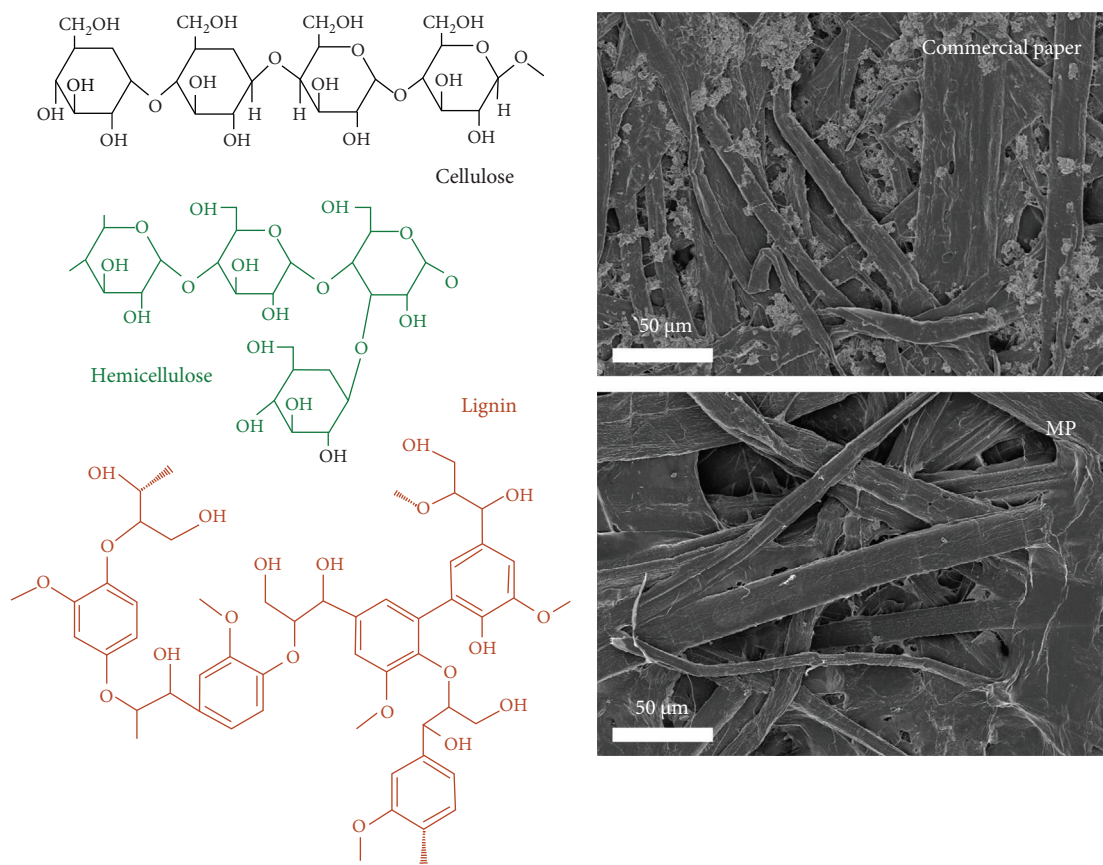
and the power density (P) was calculated using Equation (11):

$$P = \frac{3600E}{\Delta t}. \quad (11)$$

3. Results and Discussion

3.1. Characteristics of the MP. As with the typical commercial paper, the as-fabricated MP is derived from wood materials, which generally consist of cellulose, holocellulose, and lignin (Figure 3a). The surface morphology, mechanical strength, hydrophilicity, and surface chemistry of the MP and commercial paper are compared by the SEM images, tensile test results, contact angle measurements, and XPS analyses in Figure 3b–e. First, the SEM images in Figure 3b indicate that the MP has thicker and longer fibers than the commercial paper. These fibers are expected to contribute to mechanical strength due to strong network formation via van der Waals forces. Indeed, the stress–strain curves in Figure 3c demonstrate that the MP exhibits superior mechanical strength to that of the commercial paper.

With respect to the wettability, the results in Figure 3d indicate that the droplet on the MP has a contact angle of 93.2° and is rapidly absorbed after only 12 s, whereas the initial contact angle on the commercial paper is 100.4° and shows little change (to 100.1°) after 60 s. Finally, the chemical compositions of the MP and commercial paper are confirmed by



(c)

FIGURE 3: Continued.

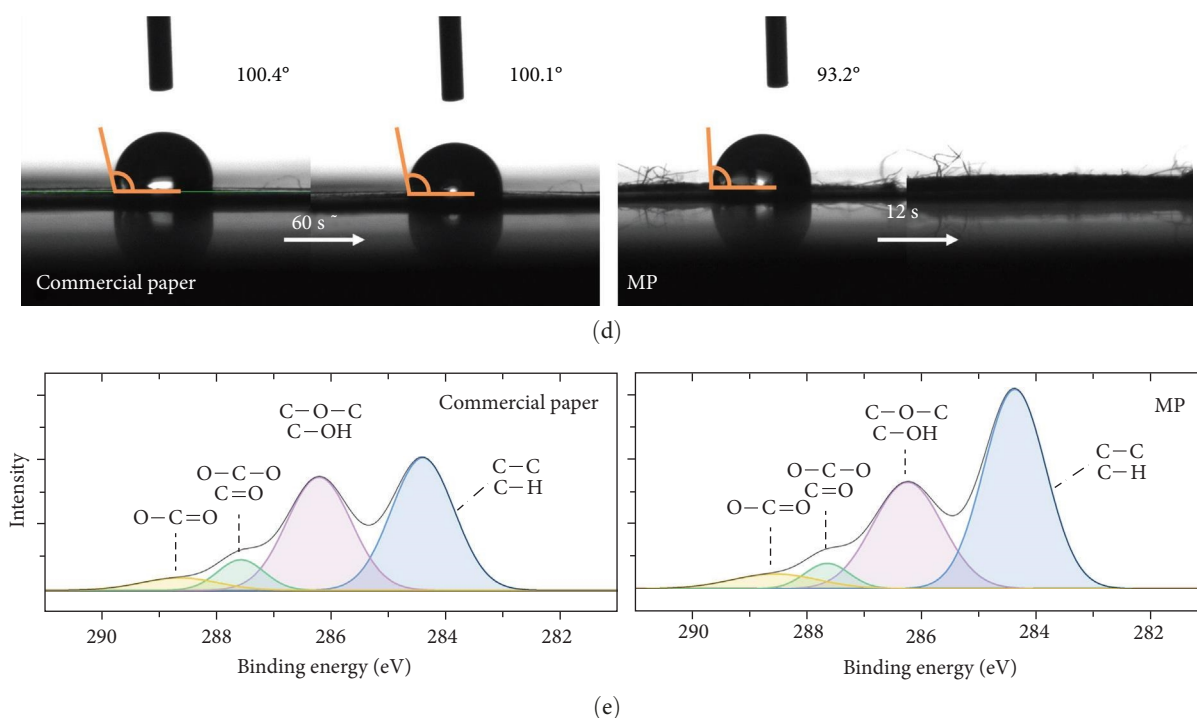


FIGURE 3: (a) The chemical structures of the various components of paper, the comparative SEM images (b), stress–strain curves (c), contact angle measurements (d), and X-ray photoelectron spectroscopy (XPS) profiles (e) of the commercial paper and mulberry paper (MP).

the XPS results in Figure 3e. Here, the abundant —OH , C—O—C , and C—H bonds of holocellulose (the mixture of cellulose and hemicellulose) appear as larger peaks in the MP, while the commercial paper exhibits a larger peak at 287.7 eV due to the C=O group, which is the primary bonding component in lignin. These results indicate that the MP has a higher holocellulose content and lower lignin content than the commercial paper. The —OH functional groups in the holocellulose structure contribute to hydrophilicity and provide hydrogen-bonding sites, thereby, increasing the mechanical strength and the wettability of the paper. These results confirm that the MP exhibits superior adhesion with active materials due to its excellent wettability [27], attributed to its inherent characteristics. Therefore, the MP with high holocellulose content is a powerful candidate for use as a substrate for flexible electrodes.

3.2. Characteristics of OPAC. The chemical compositions and surface properties of the dried OP and OPAC are revealed by the EDS results, FE-SEM images, and BET analyses in Tables S1 and S2 and Figure 4. The dried OP contains 82.79 at% carbon (C), along with some nitrogen (N) and oxygen (O), while the carbon content of the OPAC increased to 93.08 at%, with corresponding decreases in the other components, due to proper pre-carbonization and activation (Table S1). Moreover, the FE-SEM image of the OP powder indicates a randomly rough surface without any clear structure (Figure 4a), while the OPAC powder exhibits a well-developed pore structure due to KOH activation (Figure 4b). These results are further confirmed by the BET isothermal analyses in Figure 4c,d and Table S2. Here, the total pore volume (V_{total}) significantly increased from 0.00343 to 0.639 cm^3/g after activation. The

BET surface area (S_{BET}) is also seen to have increased dramatically from 1.774 m^2/g for the OP to 986.010 m^2/g for the OPAC. The expanded porosity and surface area contributes to rise in EDL capacitance. Moreover, the development of mesopores in the OPAC is indicated by its adsorption and desorption average pore diameter (APD) values of 2.496 and 2.688 nm, respectively, compared to 6.435 and 9.016 nm for the OP. The mesopore diameter of the as-prepared OPAC is advantageous for application as an EDL capacitive material because it facilitates ion adsorption on the surface, which would be hindered in micropores of less than 2 nm.

3.3. Characteristics of the MP-Based Electrode With the Hybrid Nanocomposite Coating. The successful coating of active materials is confirmed by the FE-SEM images in Figure 5. The microscale mulberry fibers of the bare MP are clearly observed in Figure 5a and such fibers are seen to cover the OPAC0@MP and OPAC20@MP in Figure 5b,c. At higher magnification, the OPAC0@MP, which contains no OPAC, exhibits only densely coated CNT fibers on the mulberry fibers (Figure 5d), while the OPAC20@MP exhibits a coarse porous surface (Figure 5e). This result demonstrates that the OPAC not only has a porous structure by itself, but also enables the fabrication of an electrode with large surface area. Moreover, the top-view FE-SEM image of the PEDOT:PSS/OPAC@MP electrode in Figure 5f demonstrates the formation of thick layer of PEDOT:PSS due to the polymer property.

The coating of OPAC and PEDOT:PSS is further confirmed by the XPS results for the bare MP, the OPAC@MP, and the PEDOT:PSS/OPAC@MP in Figure 6 and Figure S1. Thus, in the full survey spectra (Figure S1), the bare MP exhibits primary peaks due to the C 1s and O 1s, while a minor S 2p

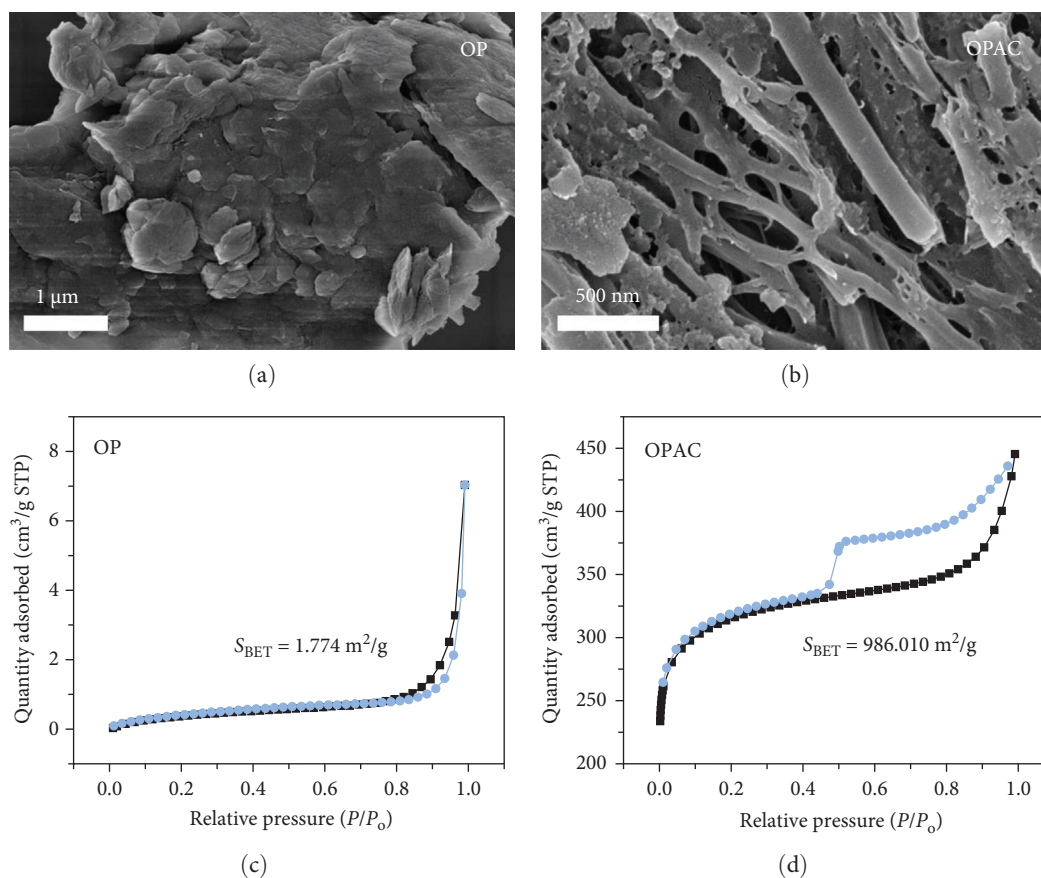


FIGURE 4: The top-view field-emission scanning electron microscopy (FE-SEM) images (a and b) and isothermal analyses (c and d) of the dried orange peel (OP) (a and c) and OP-derived activated carbon (OPAC) (b and d).

peak appears after coating with OPAC due to the SDBS surfactant in the OPAC ink. Moreover, the intensity of the S 2p peak is notably increased after coating with PEDOT:PSS, which can be attributed to the sulfur atoms and sulfonate groups of PEDOT:PSS.

In further detail, the C 1s peak of the bare MP can be split into several peaks located at 284.4, 286.2, and 287.4 eV (Figure 6a), which correspond to the C=C, C—O/C—S, and C=O bonds, respectively. After coating with OPAC, the C 1s peak is resolved into components corresponding to C=C, C—C, and C=O bonds at binding energies of 284.4, 285.2, and 287.0 eV, respectively. Further, after coating with PEDOT:PSS, the C 1s peak is simplified so that the split peak shows components corresponding to C=C at 284.4 eV and C—N/C—S at 285.7 eV, which is consistent with previous study [4].

Consistently with the overall XPS results (Figure S1), no S 2p peak appears in the bare MP (Figure 6a), while low-intensity S 2p peaks appear at 168.5 and 170 eV after coating with OPAC (Figure 6b). These peaks originate from SDBS, which was used as a surfactant in the OPAC ink. The molecular structure of SDBS is shown in Figure 6b. After additional coating with PEDOT:PSS, the S 2p peak separates into two peaks, representing the PEDOT and PSS groups (Figure 6c). The PEDOT group is further deconvoluted into peaks corresponding to the PEDOT 2p_{3/2} and PEDOT 2p_{1/2} at 163.4 and 164.8 eV, while the PSS group is deconvoluted into two peaks at 167.8 and

168.8 eV, corresponding to the PSS 2p_{3/2} and PSS 2p_{1/2}, respectively [22, 28, 29].

3.4. Electrochemical Measurements. The optimal ratio between the EDL capacitive material (OPAC) and conductive additive (CNTs) can be identified by comparing the capacitance values calculated using the CV and CD curves of the various OPAC@MP samples in Figure 7a,b. Here, the curve area and discharge time are seen to increase as the mass of OPAC increases, thereby, resulting in higher capacitance. Consequently, the areal capacitances calculated using the CV and CD curves are shown in Table S3 and Figure 7c,d. As the mass of OPAC increases, the capacitances tend to rise, reaching highest value with OPAC30@MP. However, between OPAC20 and OPAC30, the performance improvement is minimal relative to the increase in mass of active materials, suggesting saturation state. This result is attributed to low electric conductivity of OPAC compared to CNT. Therefore, OPAC20@MP can be considered as the most favorable electrode with a C_s and C_{CD} of 36.23 ± 3.46 and 18.25 ± 1.09 mF/cm², respectively, compared to 4.18 ± 1.38 and 1.69 ± 0.18 mF/cm², respectively, for the OPAC0@MP. Therefore, the OPAC20 dispersion was utilized in subsequent experiments and electrochemical measurements to prepare OPAC@MP and PEDOT:PSS/OPAC@MP electrodes.

For the electrochemical measurements, symmetric supercapacitors were fabricated using either the OPAC@MP or the

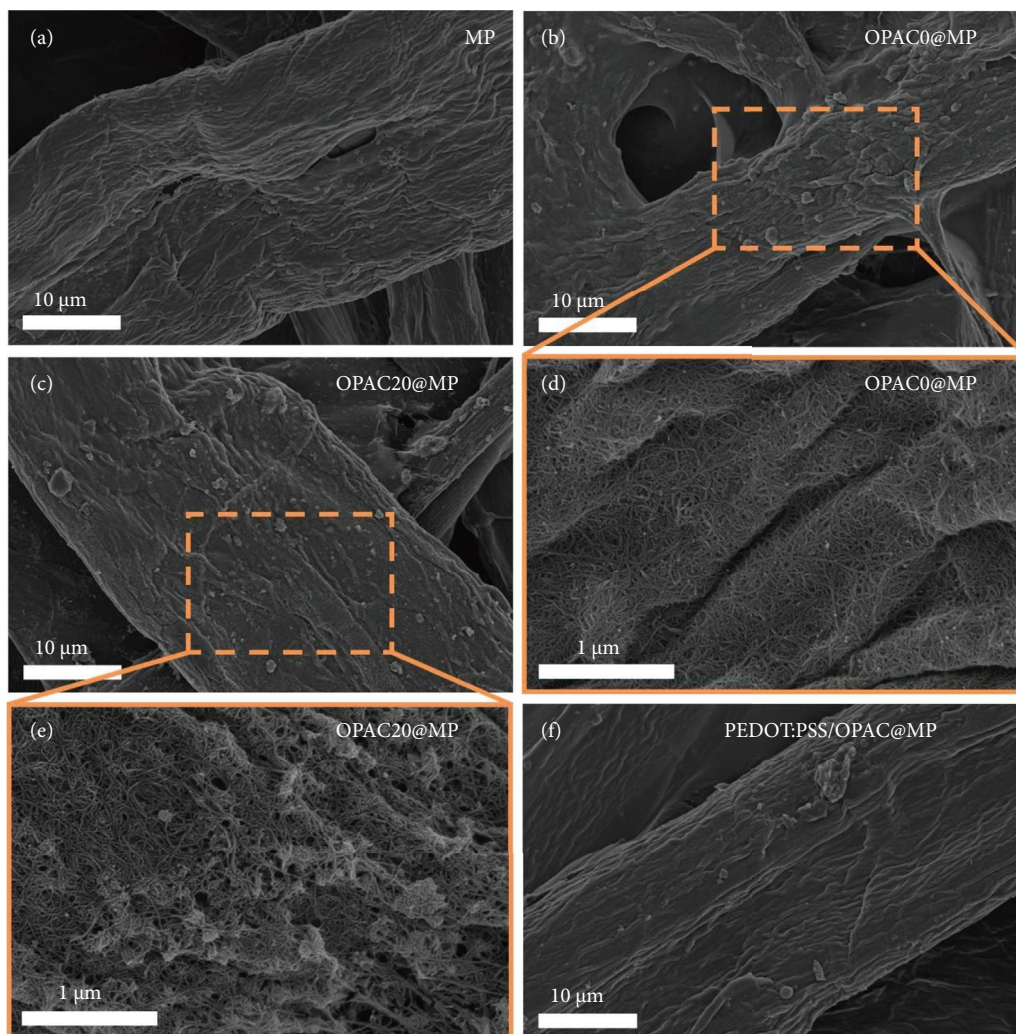


FIGURE 5: The top-view field-emission scanning electron microscopy (FE-SEM) images of (a) the bare MP, (b) the OPAC0@MP, and (c) the OPAC20@MP. (d and e) High-resolution images of the areas indicated by the red squares in (b) and (c), respectively. (f) The top-view FE-SEM image of the PEDOT:PSS/OPAC@MP. MP, mulberry paper; OPAC, orange peel-derived activated carbon; PEDOT, poly(3,4-ethylenedioxythiophene); PSS, polystyrene sulfonate.

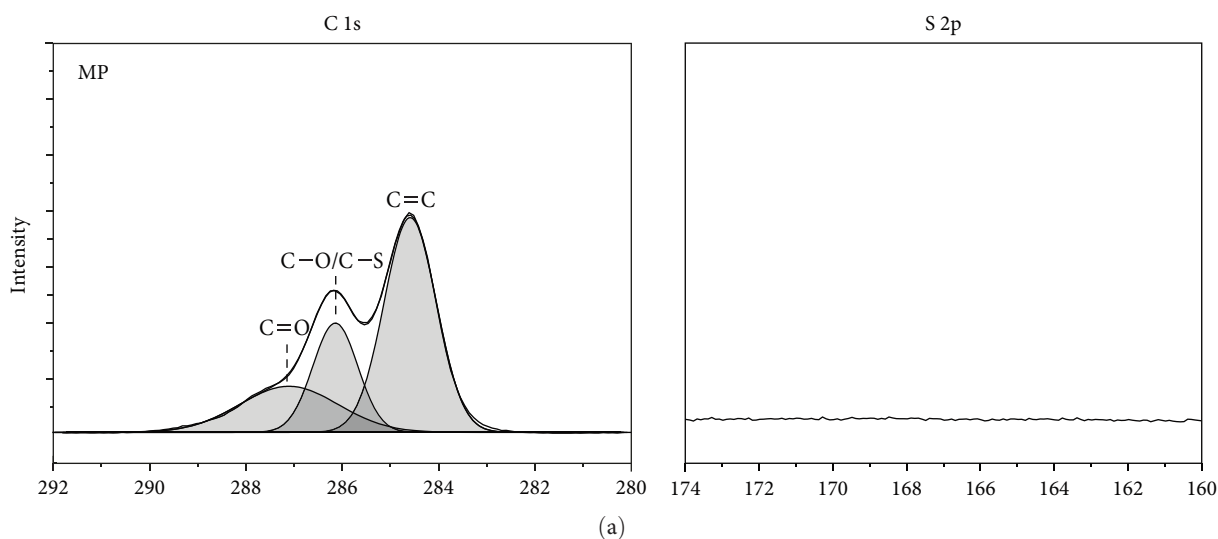


FIGURE 6: Continued.

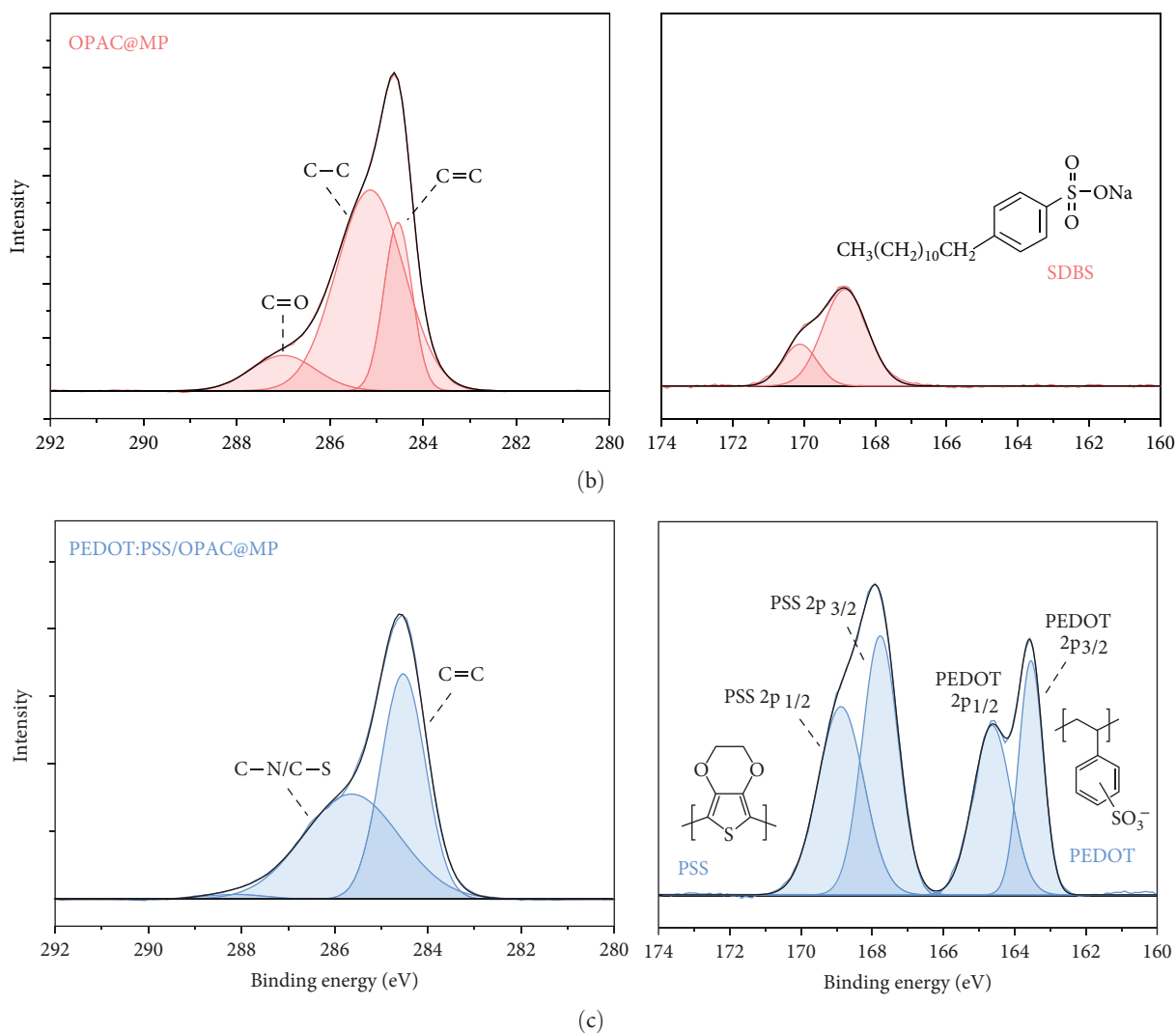


FIGURE 6: The C 1s and S 2p X-ray photoelectron spectroscopy (XPS) profiles of (a) the bare MP, (b) the OPAC@MP, and (c) the PEDOT:PSS/OPAC@MP. MP, mulberry paper; OPAC, orange peel-derived activated carbon; PEDOT, poly(3,4-ethylenedioxythiophene); PSS, polystyrene sulfonate.

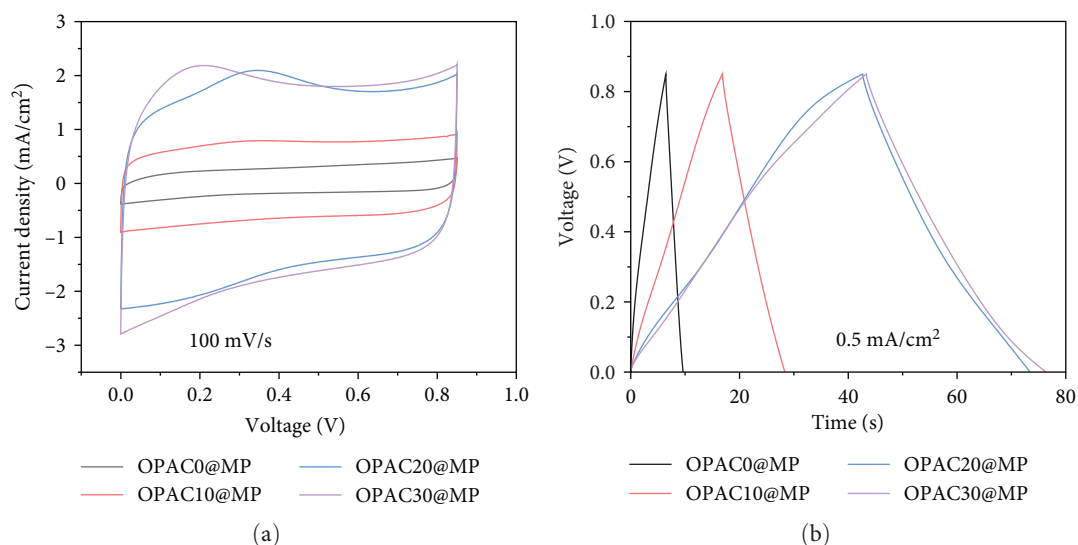


FIGURE 7: Continued.

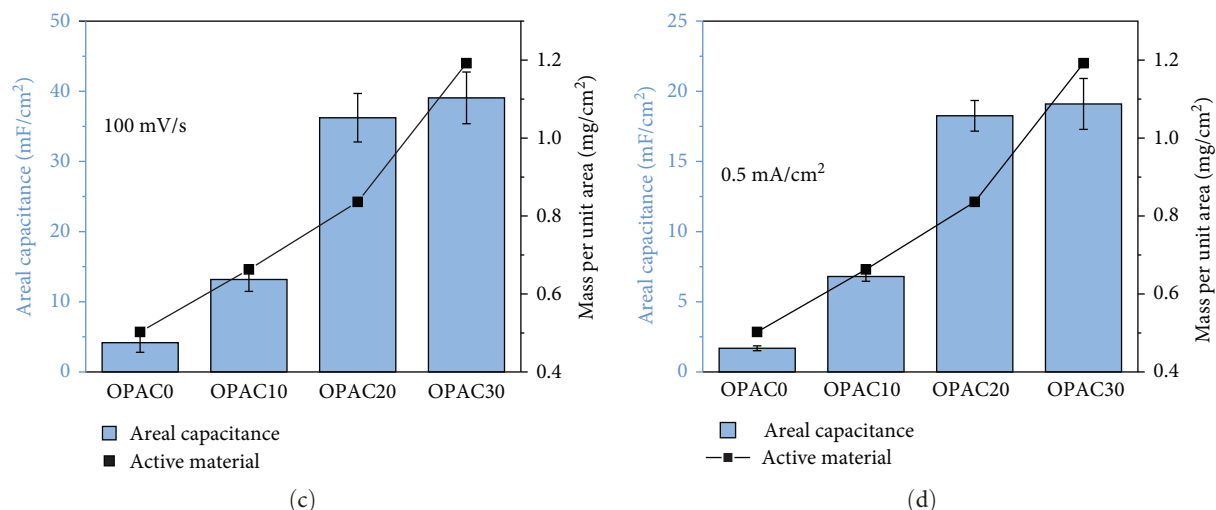


FIGURE 7: The electrochemical measurement results for the various OPAC@MP materials: (a) the cyclic voltammetry (CV) curves obtained at a scan rate of 100 mV/s, (b) the charge–discharge (CD) curves obtained at a current density of 0.5 mA/cm², (c and d) the corresponding calculated areal capacitance values for (a) and (b), respectively. MP, mulberry paper; OPAC, orange peel-derived activated carbon.

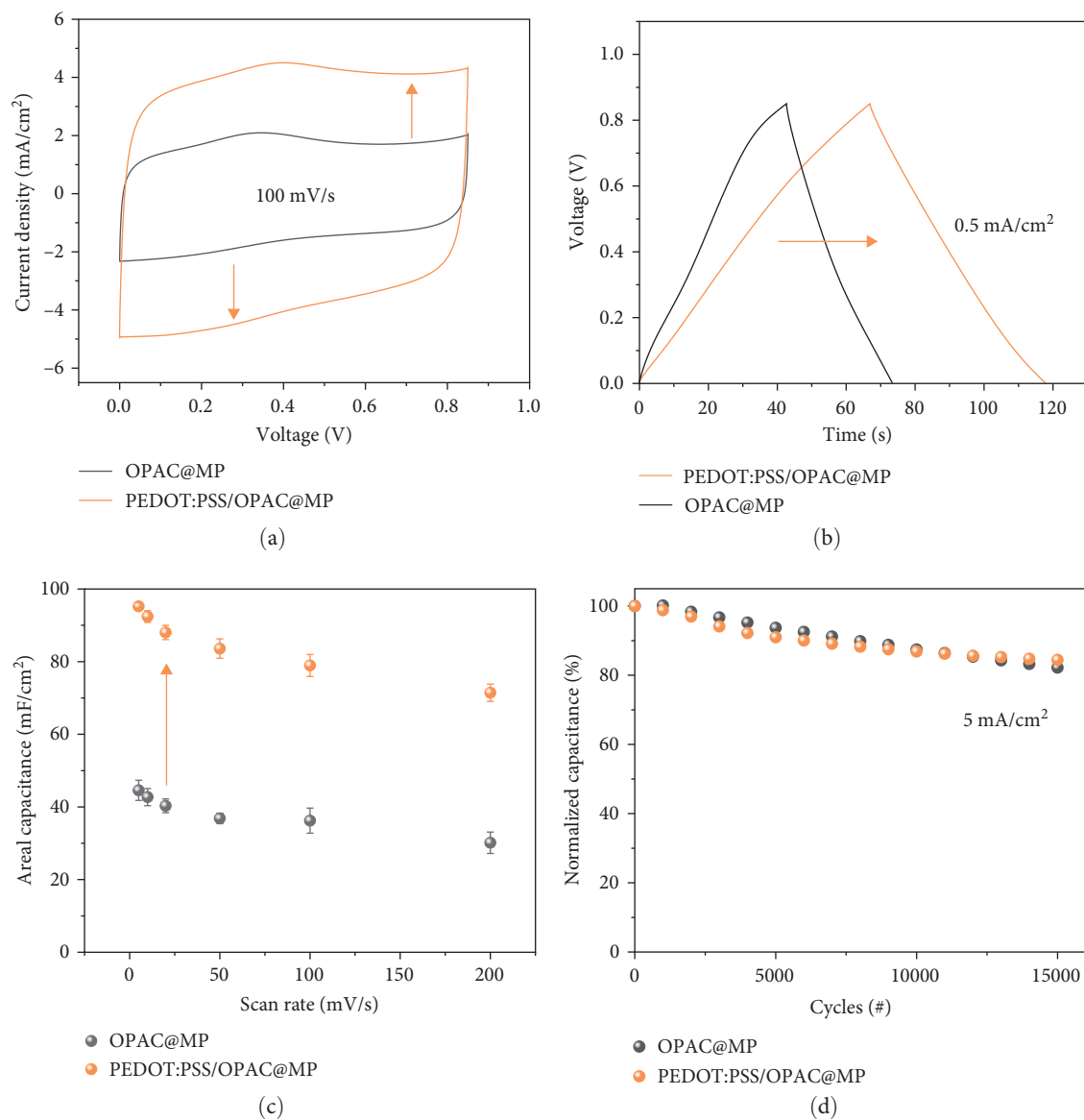


FIGURE 8: Continued.

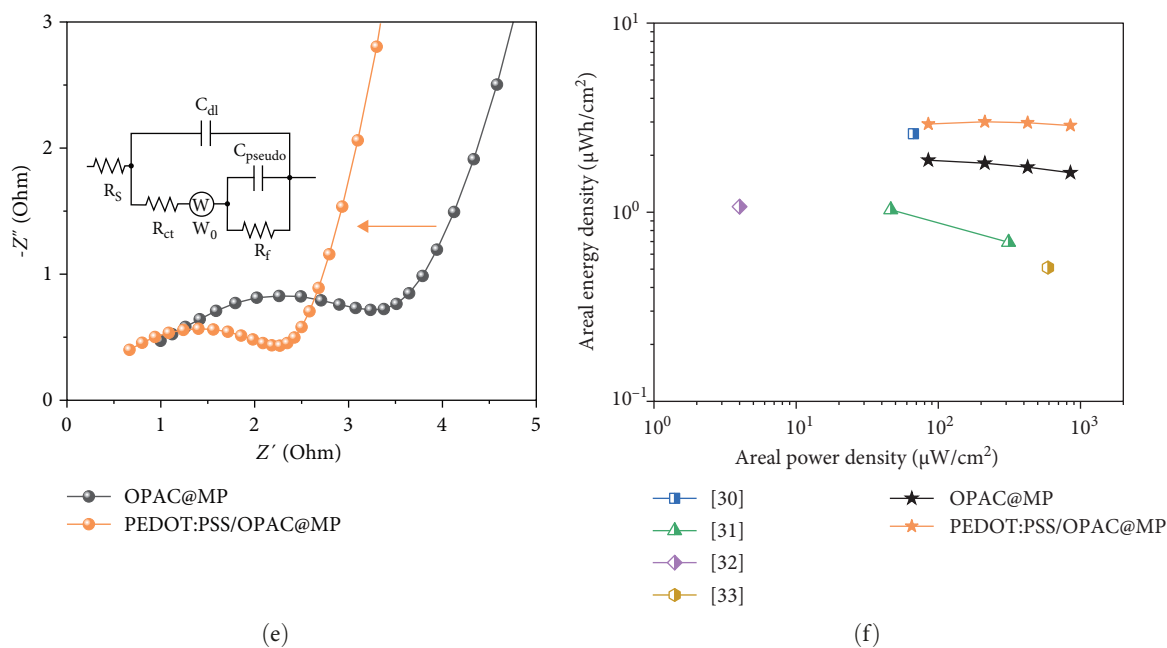


FIGURE 8: The electrochemical measurement results for the OPAC@MP and PEDOT:PSS/OPAC@MP samples: (a) the cyclic voltammetry (CV) curves, (b) the charge–discharge (CD) curves, (c) the areal capacitances calculated using the CV curve under various scan rates, (d) the cyclic stability during 15,000 cycles, (e) the electrochemical impedance (EI) Nyquist plot, and (f) the Ragone plots compared with previous studies [30–33]. Inset in (e) is the equivalent circuit for the Nyquist plot. MP, mulberry paper; OPAC, orange peel-derived activated carbon; PEDOT, poly(3,4-ethylenedioxythiophene); PSS, polystyrene sulfonate.

optimized PEDOT:PSS/OPAC@MP electrode by using a coin cell system. The electrode and separator were soaked in 1 M H_2SO_4 electrolyte and stacked in the coin cell can in the following order: electrode, separator, electrode, spacer, and spring. The stack was then capped with the coin cell cap. The electrochemical performances of these supercapacitors are compared via the corresponding CV and CD curves obtained under scan rate of 100 mV/s and current densities of 0.5 mA/cm² in Figure 8a,b. Here, the curve area and discharge time are seen to increase with the additional coating of PEDOT:PSS. Using Equations ((8) and ((9), the enlarged curve area and prolonged discharge time are found to contribute to higher capacitances (C_S and C_{CD}) calculated from the respective CV and CD curves. Thus, in Figure 8c and Table S4, the PEDOT:PSS/OPAC@MP exhibits C_S values that are approximately 2.3 times higher than those of the OPAC@MP under each scan rate. For example, at a scan rate of 100 mV/s, the PEDOT:PSS/OPAC@MP electrode exhibits a C_S of 78.95 ± 3.04 mF/cm² compared to 36.23 ± 1.42 mF/cm² for the OPAC@MP. Moreover, from Equation (10), the energy density (E) is increased by 66%, from 1.81 to 3.01 $\mu\text{W h}/\text{cm}^2$ (at a current density of 0.5 mA/cm²) for the OPAC@MP and PEDOT:PSS/OPAC@MP, respectively, thereby, indicating that coating with the pseudocapacitive PEDOT:PSS enhances the low energy density of the EDL capacitive material.

In addition, the cyclic stability of each supercapacitor was measured during 15,000 cycles at a current density of 5 mA/cm², and the results are presented in Figure 8d. Here, the cyclic stability is seen to be improved after coating with PEDOT:PSS, especially after 10,000 cycles. This is because the PEDOT:PSS

layer prevents delamination of the carbon-based materials so that the PEDOT:PSS/OPAC@MP is reliable for long-term use with excellent capacitance retention of 84.4% after 15,000 cycles, which is excellent compared to previous studies using biomass-derived AC [34–38]. Further, the electrical conductivity of each supercapacitor is evaluated by the electrochemical impedance (EI) measurements in Figure 8e. Here, the Nyquist plots indicate that the electrical conductivity of the PEDOT:PSS/OPAC@MP device increased relative to that of the OPAC@MP device, as indicated by a lowering of the inflection point of the equivalent series resistance. This, in turn, leads to an enhanced energy density for the PEDOT:PSS/OPAC@MP even compared with previous studies (Figure 8f).

4. Conclusions

Herein, organic-based materials were prepared from OPAC, and the optimized material was used to fabricate MP-based electrode for use in a flexible supercapacitor. The OPAC was fabricated via HTC followed by activation with KOH, which is a well-known method for preparing AC from organic waste. Due to this sequential fabrication procedure, the OPAC developed a pore structure and increased carbon content, thus, resulting in an increased specific surface area (S_{BET}) and total pore volume (V_{total}) of the OPAC were 986.010 m²/g and 0.639 cm³/g, respectively (1.774 m²/g and 0.00343 cm³/g for the OP). Therefore, the prepared OPAC exhibits enhanced properties for capacitive behavior based on EDL and the precursor from nature provide sustainability and eco-friendliness as well as cost effectiveness in practical view.

With regard to the coating of the MP with the active material, the OPAC ink was prepared in various mass ratios of CNT: OPAC (1:0, 1:10, 1:20, and 1:30) and the optimal ratio was found to be 1:20. The optimal OPAC20@MP electrode exhibited a specific capacitance of $36.23 \pm 3.46 \text{ mF/cm}^2$ according to CV at a scan rate of 100 mV/s and a specific capacitance of $18.25 \pm 1.09 \text{ mF/cm}^2$ according to the CD curve at a current density of 0.5 mA/cm^2 . These capacitance values were extremely higher than those of the OPAC0@MP (4.18 ± 1.38 and $1.69 \pm 0.18 \text{ mF/cm}^2$, respectively), due to the increased surface area and pore structure, which enabled more energy to be stored.

Subsequently, the optimal OPAC20@MP electrode was dipped in PEDOT:PSS solution to provide enhanced capacitance and energy density. Electrochemical measurements indicated that the resulting PEDOT:PSS/OPAC@MP electrode exhibited a specific capacitance of $78.95 \pm 3.04 \text{ mF/cm}^2$ according to CV at a scan rate of 100 mV/s , which represents an increase of about 2.3 times compared to that of the OPAC@MP ($36.23 \pm 1.42 \text{ mF/cm}^2$). Moreover, the energy density (E) was increased from 1.81 to $3.01 \mu\text{Wh/cm}^2$ after extra coating of PEDOT:PSS, thereby, demonstrating that pseudocapacitive material improved the low energy density of the EDL capacitive material.

In brief, the present paper concentrated on the effective preparation of organic-derived AC and evaluated the electrochemical performance of the as-fabricated PEDOT:PSS/OPAC@MP electrode. This investigation proposes sustainable and eco-friendly electrodes by combining AC and MP, derived from recycling biowaste and biodegradable substrates with flexibility, respectively. Furthermore, this electrode, with a hybrid coating of EDL capacitive and pseudocapacitive materials, has potential applications in next-generation energy storage systems, providing increased capacitance and enhanced energy density due to the synergistic effect. The demonstrated results are expected to broaden the possibilities for advanced energy materials, opening avenues for future research on the scalability and employment of various precursors, which should be addressed.

Data Availability Statement

The data that support the findings of this study are available on request from the corresponding author. The data are not publicly available due to privacy or ethical restrictions.

Ethics Statement

The authors have nothing to report.

Consent

The authors have nothing to report.

Conflicts of Interest

The authors declare no conflicts of interest.

Author Contributions

All the authors contributed to the conception and design of the study. Data collection and data analysis were performed by Yurim Han, Hyungsub Yoon, and Byungil Hwang. The first draft of the manuscript was written by Yurim Han, Jun Young Cheong, and Byungil Hwang, and all the authors commented on the current version of the manuscript. All the authors have read and approved the final manuscript.

Funding

This research was supported by GRDC (Global Research Development Center) Cooperative Hub Program through the National Research Foundation of Korea (NRF) funded by the Ministry of Science and ICT (MSIT) (RS-2023-00257595).

Supporting Information

Additional supporting information can be found online in the Supporting Information section. (*Supporting Information*) Figure S1 presents the full survey XPS results for bare MP, OPAC@MP, and PEDOT:PSS/OPAC@MP. Tables S1 and S2 summarize the EDS and BET analyses of dried OP and OPAC. Tables S3 and S4 provide specific values for electrochemical performance.

References

- [1] T. G. Yun, D. Kim, S. M. Kim, I. D. Kim, S. Hyun, and S. M. Han, "Mulberry Paper-Based Supercapacitor Exhibiting High Mechanical and Chemical Toughness for Large-Scale Energy Storage Applications," *Advanced Energy Materials* 8, no. 21 (2018): 1800064.
- [2] Y. Li, Y. Zhang, J. Gao, S. Liao, and G. Zhang, "Polyethylene Terephthalate Fiber Modified With Type I Collagen as a 3D Scaffold Material for Bioartificial Liver," *Applied Sciences* 14, no. 11 (2024): 4537.
- [3] J. Zhu, Y. Tian, C. Yang, et al., "Low-Cost and Fast Fabrication of the Ultrasonic Embossing on Polyethylene Terephthalate (PET) Films Using Laser Processed Molds," *Microsystem Technologies* 23, no. 12 (2017): 5653–5668.
- [4] Y. Han, H. Ha, T. Suryaprabha, P. Baumli, and B. Hwang, "Mulberry-Paper-Based Electrodes With Hybrid Nanocomposite Coatings and Their Application to Eco-Friendly Energy-Storage Devices," *Cellulose* 31, no. 3 (2024): 1675–1685.
- [5] M. Govindasamy, S. Shanthi, E. Elaiyappillai, et al., "Fabrication of Hierarchical NiCo₂S₄@CoS₂ Nanostructures on Highly Conductive Flexible Carbon Cloth Substrate as a Hybrid Electrode Material for Supercapacitors With Enhanced Electrochemical Performance," *Electrochimica Acta* 293 (2019): 328–337.
- [6] Z. Li, D. Guo, Y. Liu, H. Wang, and L. Wang, "Recent Advances and Challenges in Biomass-Derived Porous Carbon Nanomaterials for Supercapacitors," *Chemical Engineering Journal* 397 (2020): 125418.
- [7] J. Gamby, P. L. Taberna, P. Simon, J. F. Fauvarque, and M. Chesneau, "Studies and Characterisations of Various Activated Carbons Used for Carbon/Carbon Supercapacitors," *Journal of Power Sources* 101, no. 1 (2001): 109–116.
- [8] C. Lei, N. Amini, F. Markoulidis, P. Wilson, S. Tennison, and C. Lekakou, "Activated Carbon From Phenolic Resin With Controlled Mesoporosity for an Electric Double-Layer Capacitor

- (EDLC),” *Journal of Materials Chemistry A* 1, no. 19 (2013): 6037–6042.
- [9] Q.-S. Liu, T. Zheng, P. Wang, and L. Guo, “Preparation and Characterization of Activated Carbon From Bamboo by Microwave-Induced Phosphoric Acid Activation,” *Industrial Crops and Products* 31, no. 2 (2010): 233–238.
- [10] Z. Hu and M. P. Srinivasan, “Mesoporous High-Surface-Area Activated Carbon,” *Microporous and Mesoporous Materials* 43, no. 3 (2001): 267–275.
- [11] E. Y. L. Teo, L. Muniandy, E.-P. Ng, et al., “High Surface Area Activated Carbon From Rice Husk as a High Performance Supercapacitor Electrode,” *Electrochimica Acta* 192 (2016): 110–119.
- [12] A. Kamińska, P. Miądlicki, K. Kiełbasa, et al., “Activated Carbons Obtained From Orange Peels, Coffee Grounds, and Sunflower Husks—Comparison of Physicochemical Properties and Activity in the Alpha-Pinene Isomerization Process,” *Materials* 14, no. 23 (2021): 7448.
- [13] H. H. Kim, R. H. Park, and Y. J. Kim, “Preparation of Activated Carbons Using Biomass,” *Journal of the Korean Industrial and Engineering Chemistry* 15 (2004): 870–874.
- [14] N. A. Rashidi, Y. H. Chai, I. S. Ismail, M. F. H. Othman, and S. Yusup, “Biomass as Activated Carbon Precursor and Potential in Supercapacitor Applications,” *Biomass Conversion and Biorefinery* (2022): 1–15.
- [15] B. Li, F. Dai, Q. Xiao, et al., “Activated Carbon From Biomass Transfer for High-Energy Density Lithium-Ion Supercapacitors,” *Advanced Energy Materials* 6, no. 18 (2016): 1600802.
- [16] İ. Demiral, C. Samdan, and H. Demiral, “Enrichment of the Surface Functional Groups of Activated Carbon by Modification Method,” *Surfaces and Interfaces* 22 (2021): 100873.
- [17] E. Köseoğlu and C. Akmil-Başar, “Preparation, Structural Evaluation and Adsorptive Properties of Activated Carbon From Agricultural Waste Biomass,” *Advanced Powder Technology* 26, no. 3 (2015): 811–818.
- [18] A. Singh and A. K. Ojha, “Orange Peel Derived Activated Carbon for Supercapacitor Electrode Material,” *Journal of Materials Science: Materials in Electronics* 34 (2023): 1003.
- [19] S. Żółtowska, I. Koltsov, K. Alejski, H. Ehrlich, M. Ciałkowski, and T. Jesionowski, “Thermal Decomposition Behaviour and Numerical Fitting for the Pyrolysis Kinetics of 3D Spongin-Based Scaffolds. The Classic Approach,” *Polymer Testing* 97 (2021): 107148.
- [20] S. M. Omokafe, A. A. Adeniyi, E. O. Igbafen, S. R. Oke, and P. A. Olubambi, “Fabrication of Activated Carbon From Coconut Shells and Its Electrochemical Properties for Supercapacitors,” *International Journal of Electrochemical Science* 15, no. 11 (2020): 10854–10865.
- [21] C. Dai, J. Wan, J. Shao, and F. Ma, “Hollow Activated Carbon With Unique through-Pore Structure Derived From Reed Straw for High-Performance Supercapacitors,” *Materials Letters* 193 (2017): 279–282.
- [22] Y. Seo, H. Ha, J. Y. Cheong, et al., “Highly Reliable Yarn-Type Supercapacitor Using Conductive Silk Yarns With Multilayered Active Materials,” *Journal of Natural Fibers* 19, no. 3 (2022): 835–846.
- [23] L. Guan, L. Yu, and G. Z. Chen, “Capacitive and Non-Capacitive Faradaic Charge Storage,” *Electrochimica Acta* 206 (2016): 464–478.
- [24] L. Zuo, J. Ai, H. Fu, et al., “Enhanced Removal of Sulfonamide Antibiotics by KOH-Activated Anthracite Coal: Batch and Fixed-Bed Studies,” *Environmental Pollution* 211 (2016): 425–434.
- [25] Z. Heidarinejad, M. H. Dehghani, M. Heidari, G. Javedan, I. Ali, and M. Sillanpää, “Methods for Preparation and Activation of Activated Carbon: A Review,” *Environmental Chemistry Letters* 18, no. 2 (2020): 393–415.
- [26] M. A. Chayid and M. J. Ahmed, “Amoxicillin Adsorption on Microwave Prepared Activated Carbon From *Arundo donax* Linn: Isotherms, Kinetics, and Thermodynamics Studies,” *Journal of Environmental Chemical Engineering* 3, no. 3 (2015): 1592–1601.
- [27] C. Zhang, L. Gong, L. Xiang, et al., “Deposition and Adhesion of Polydopamine on the Surfaces of Varying Wettability,” *ACS Applied Materials & Interfaces* 9, no. 36 (2017): 30943–30950.
- [28] H. M. Lee, G. Anoop, H. J. Lee, W. S. Kim, and J. Y. Jo, “Key Parameters for Enhancing the Thermoelectric Power Factor of PEDOT: PSS/PANI-CSA Multilayer Thin Films,” *RSC Advances* 9, no. 21 (2019): 11595–11601.
- [29] T. A. Yemata, Y. Zheng, A. K. K. Kyaw, et al., “Modulation of the Doping Level of PEDOT: PSS Film by Treatment With Hydrazine to Improve the Seebeck Coefficient,” *RSC Advances* 10, no. 3 (2020): 1786–1792.
- [30] C. Choi, S. H. Kim, H. J. Sim, et al., “Stretchable, Weavable Coiled Carbon Nanotube/MnO₂/Polymer Fiber Solid-State Supercapacitors,” *Scientific Reports* 5, no. 1 (2015): 9387.
- [31] X. Shi, Z. Zeng, C. Liao, et al., “Flexible, Planar Integratable and All-Solid-State Micro-Supercapacitors Based on Nanoporous Gold/Manganese Oxide Hybrid Electrodes via Template Plasma Etching Method,” *Journal of Alloys and Compounds* 739 (2018): 979–986.
- [32] H. Chen, S. Chen, Y. Zhang, H. Ren, X. Hu, and Y. Bai, “Sand-Milling Fabrication of Screen-Printable Graphene Composite Inks for High-Performance Planar Micro-Supercapacitors,” *ACS Applied Materials & Interfaces* 12, no. 50 (2020): 56319–56329.
- [33] A. Jo, S.-i. Chung, P. K. Kim, et al., “All-Printed Paper-Based Micro-Supercapacitors Using Water-Based Additive-Free Oxidized Single-Walled Carbon Nanotube Pastes,” *ACS Applied Energy Materials* 4, no. 12 (2021): 13666–13675.
- [34] X. Han, H. Jiang, Y. Zhou, et al., “A High Performance Nitrogen-Doped Porous Activated Carbon for Supercapacitor Derived From Pueraria,” *Journal of Alloys and Compounds* 744 (2018): 544–551.
- [35] A. Jain, C. Xu, S. Jayaraman, R. Balasubramanian, J. Y. Lee, and M. P. Srinivasan, “Mesoporous Activated Carbons With Enhanced Porosity by Optimal Hydrothermal Pre-Treatment of Biomass for Supercapacitor Applications,” *Microporous and Mesoporous Materials* 218 (2015): 55–61.
- [36] I. I. Misnon, N. K. M. Zain, R. A. Aziz, B. Vidyadharan, and R. Jose, “Electrochemical Properties of Carbon From Oil Palm Kernel Shell for High Performance Supercapacitors,” *Electrochimica Acta* 174 (2015): 78–86.
- [37] C. Peng, X.-B. Yan, R.-T. Wang, J.-W. Lang, Y.-J. Ou, and Q.-J. Xue, “Promising Activated Carbons Derived From Waste Tea-Leaves and Their Application in High Performance Supercapacitors Electrodes,” *Electrochimica Acta* 87 (2013): 401–408.
- [38] D. Wang, S. Liu, G. Fang, G. Geng, and J. Ma, “From Trash to Treasure: Direct Transformation of Onion Husks Into Three-Dimensional Interconnected Porous Carbon Frameworks for High-Performance Supercapacitors in Organic Electrolyte,” *Electrochimica Acta* 216 (2016): 405–411.